# Optimization of a Lumped Element Circulator Based on Eigenvalue Evaluation and Structural Improvement

Taro Miura, Makoto Kobayashi, and Yoshihiro Konishi, *Fellow, IEEE*

***Abstract*—An optimization technique for a lumped element circulator has been established from the point of view of theoretical characteristic design and structural improvement. A theoretical design based on the evaluation of the eigenvalues of an inductance matrix made it possible to optimize the isolation bandwidth characteristic of a structurally improved circulator. Structural optimization was achieved by the application of multilayer ceramic technology and novel conductor formation methods to increase the isolation bandwidth of the circulator and to decrease its insertion loss. The 20 dB isolation bandwidth of 5.8% obtained by this circulator exceeded the characteristics of a conventional circulator of the same size by 29%, while an insertion loss of 0.35 dB was maintained. In view of the present status of ceramic technology, it is believed that this circulator has been ultimately close to the preferred structure for lumped element circulators.**

## I. Introduction

In the case of a conventional lumped element circulator, its inductive part is constructed by two vertically magnetized ferrite disks and a trigonally symmetric driving line inserted between the disks. The RF magnetic circuit of the circulator will be discontinuous, due to a nonmagnetic air gap surrounding the driving line, which causes a demagnetizing field at the disk surface. In order to remove this discontinuity, a lumped element circulator in which the driving line is completely embedded in a magnetic material has been developed, by the application of conventional multilayer ceramic technologies [1]. This circulator has been defined as a magnetically closed circuit circulator, abbreviated as $MC^3$, due to its continuous RF magnetic circuit. A significant improvement over the performance of a conventional circulator may be expected, such as a broader-band isolation characteristic, due to an increase in tensor permeability in such a structure, which is free of demagnetizing field.

In this paper, two important aspects of the optimization of circulator characteristics are reported. The first is a theoretical design method to confirm the broader isolation bandwidth of the $MC^3$, using the eigenvalues of a measured inductance matrix, as proposed recently [2]. The relationship between the inductance matrix and the structure of the circulator driving line was analyzed by utilizing a newly developed technique for the observation of magnetic flux on a scale model of the circulator. The second aspect is novel methods for the embedding of metal conductors in the ferrite element to reduce the insertion loss of the circulator [3]. Finally, the characteristics of the $MC^3$, produced by a combination of these two aspects, are also discussed.

Manuscript received March 28, 1996.

T. Miura is with the Advanced Products Development Center, TDK Corporation, Chiba 286, Japan.

M. Kobayashi is with the Materials Research Center, TDK Corporation, Chiba 286, Japan.

Y. Konishi is with the Electronic Engineering Department, Tokyo Institute of Polytechnics, Kanagawa 243-02, Japan.

Publisher Item Identifier S 0018-9480(96)08530-4.

## II. Lumped Element Circulator Design Theory

There are two major methods for the design of a circulator, namely the scattering matrix method and the eigenvalue method. In the scattering matrix method, the transmission coefficient of the circulator is given by the product of the scattering matrix of a circulator and an input signal vector. Each element of the matrix is evaluated from the scattering coefficient between a corresponding pair of input and output ports of the circulator. This method offers great flexibility in the design a circulator, irrespective of its structure. Efforts to develop a new circulator using this method have been pursued assiduously [4].

The eigenvalue method, adopted in this paper, estimates the transmission coefficients of a circulator from the product of eigenvalues and corresponding eigenvectors. This method is appropriate for the optimization of the isolation characteristic of a lumped element circulator if the eigenvalues of the circulator inductances are known. A comprehensive design theory based on the eigenvalue method has already been established by one of the authors [5]. According to this theory, an equivalent circuit of a lossless lumped element circulator is as shown in Fig. 1. When input, output and isolated ports are defined as ports 1, 2 and 3, respectively, the transmission characteristic of a circulator $\vec{S}$ is described in terms of a scattering vector, as shown in (1), using eigenvectors $\vec{u}_i$ and reflection coefficients $s_i$, as given in (2) and (3)

$$\vec{S} = \frac{1}{3}(s_1\vec{u}_1 + s_2\vec{u}_2 + s_3\vec{u}_3) \tag{1}$$

$$\vec{u}_1 = \begin{bmatrix}1\\1\\1\end{bmatrix},\ \vec{u}_2 = \begin{bmatrix}1\\ e^{j\frac{4\pi}{3}}\\ e^{j\frac{2\pi}{3}}\end{bmatrix} \quad \text{and} \quad \vec{u}_3 = \begin{bmatrix}1\\ e^{j\frac{2\pi}{3}}\\ e^{j\frac{4\pi}{3}}\end{bmatrix} \tag{2}$$

$$s_i = \frac{y_0 - y_i}{y_0 + y_i} \tag{3}$$

where $y_0$ the characteristic admittance of the circuit and $y_i = j(\omega C - \frac{1}{\omega L_i})$ for $i = 1, 2$, and 3.

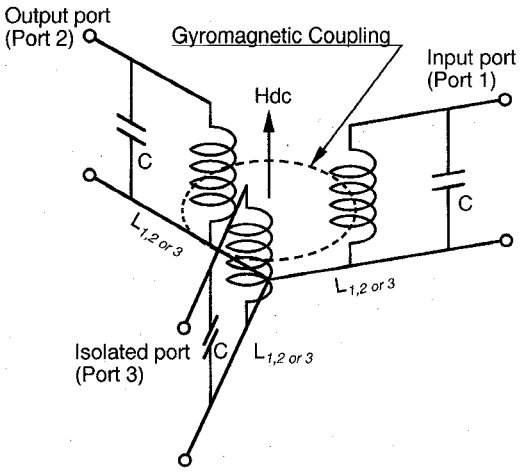


Fig. 1. Equivalent circuit of lumped element circulator.

Three inductances $L_1, L_2$, and $L_3$ in (3) are defined by the inductance of the inductive part of Fig. 1 when it is excited by the corresponding three eigenvectors. Equation (1) shows that an ideal circulator will be realized when the admittances in (3) satisfy the following conditions.

$$y_1 = \infty,\ y_2 = \frac{-j}{\sqrt{3}} \quad \text{and} \quad y_3 = \frac{j}{\sqrt{3}}.$$

The center angular frequency $\omega_r$ of the circulator is derived from the conditions above, such that is satisfies (4) and (5) simultaneously

$$\omega_r C = \frac{1}{2}\left(\frac{1}{\omega_r L_2} + \frac{1}{\omega_r L_3}\right) \tag{4}$$

$$\frac{1}{\omega_r L_3} - \frac{1}{\omega_r L_2} = \frac{2}{\sqrt{3}} y_0. \tag{5}$$

The isolation bandwidth $w_1$ of the circulator for a required isolation $S''$ is given by (6), which is derived from the transmission characteristic of the equivalent resonance circuit

$$w_1 = \frac{2\sqrt{3}|S''|\eta}{\sqrt{1+\frac{3}{4}\eta^2}}$$

where

$$\eta = \frac{L_2 - L_3}{L_2 + L_3}. \tag{6}$$

The optimization of isolation characteristics is thus reduced to the evaluation of inductance, since inductance is the only structurally dependent parameter in the circuit.

## III. Theoretical Design of Circulator Element

### A. Inductance Matrix Eigenvalue Evaluation

Previously, evaluation of the eigenvalues of the inductance matrix of a circulator has not been used in practice, due to complicated measuring procedures and the elaborate combination of phase shifters, power dividers and attenuators required for the measurement. Recently, a much simpler method for evaluating the inductances was proposed by one of the authors, utilizing eigenvectors generated in three coupled resonators, as summarized in the appendix [2]. An example of an appropriate measurement apparatus for use at 800 MHz in this experiment is shown in Fig. 2. Three quarter-wavelength dielectric resonators, of a size similar to that of the circulator sample, are attached to the sample. An input probe drives one resonator and an output probe measures the resonance output from one of the other two. By adopting this construction, the exciting vector may easily be confirmed by comparing the phase of two resonators at the resonance frequency, as has already been reported [6].

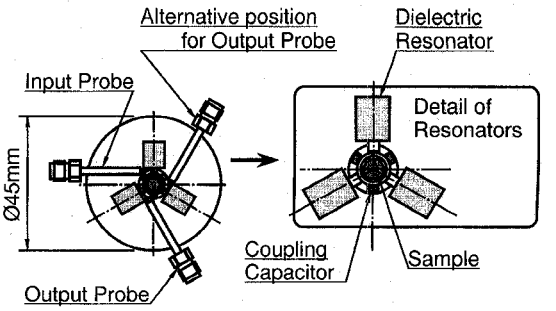


Fig. 2. Measuring jig at 800 MHz range.

It is well known that Polder's equation, shown in (7), is appropriate to describe the tensor permeability of a magnetized material as a function of an applied magnetic field and the operating frequency [7].

$$\dot{\mu}_{r\pm} = 1 + \frac{4\pi M_s}{\left(H_{\rm DC} - H_{\rm dem} \mp \frac{\omega}{\gamma}\right) + j\left(\frac{\Delta H}{2}\right)} \tag{7}$$

where $4\pi M_s$,, $H_{\rm DC}$, $H_{\rm dem}$, $\omega$, $\gamma$, and $\Delta H$ are saturation magnetization, applied DC magnetic field, demagnetizing field, angular frequency, gyromagnetic constant and ferromagnetic resonance line width, respectively. The denominator of (7) suggests that the operating frequency divided by the gyromagnetic constant is equivalent to a magnetic field. The effective magnetic field $H_{\rm eff}$, as given in (8), may thus be introduced into Polder's equation to enable data from different measurement frequencies to be plotted on one chart.

$$H_{\rm eff} = H_{\rm DC} \mp \frac{\omega}{\gamma} \tag{8}$$

where the $-$ sign is taken in the case of $L_2$ and the $+$ sign is taken for $L_3$. Fig. 3 shows an example of inductance evaluated using the method described above and in the Appendix. Measurements were taken at four frequencies, 700, 800, 900 MHz and 1 GHz, using resonators of the appropriate resonant frequency in each case. The three curves in the figure were obtained as the best fitted curves of Polder's tensor permeability equation for $L_1, L_2$ and $L_3$, respectively. The fitted expressions for the curves are given in

$$\begin{aligned}
L_1 &= 0.61\Re\left\{1 + \frac{405.7}{(H_{\rm DC} - 572.3 - \omega/\gamma) + j\cdot 25}\right\} \text{ (nH)} \\
L_2 &= 2.12\Re\left\{1 + \frac{329.9}{(H_{\rm DC} - 703.5 - \omega/\gamma) + j\cdot 25}\right\} \text{ (nH)} \\
L_3 &= 2.12\Re\left\{1 + \frac{433.9}{(H_{\rm DC} - 703.5 + \omega/\gamma) + j\cdot 25}\right\} \text{ (nH)}
\end{aligned} \tag{9}$$

where $\Re$ is the real part of the value in a bracket.

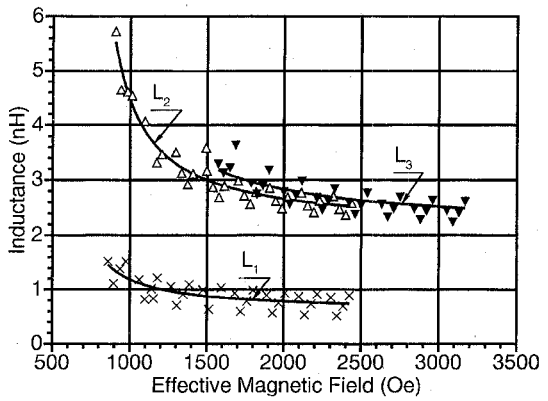


Fig. 3. Example of inductance measurement.

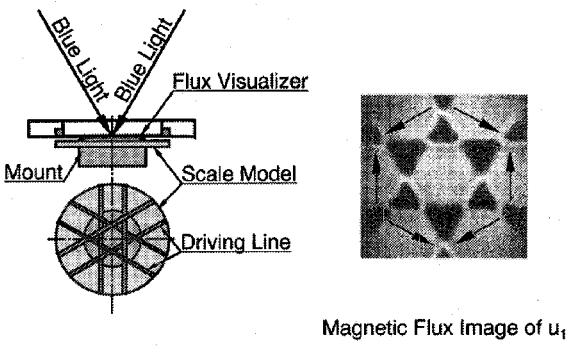


Fig. 4. Magnetic flux observing apparatus and magnetic flux image of $u_1$.

The constants in (9) were obtained by graphical fitting using a well-known graphic software. The ferromagnetic resonance line width of 50 Oe, obtained from another measurement, was substituted in the equations. These experimental results have confirmed that the inductance of the measured lumped element circulator is well described using Polder's equation.

Traditional lumped element circulator theory has assumed that each driving line will generate a uniform magnetic field in the ferrite. This assumption implies that $L_1$ should be null, due to cancellation of the flux from three lines, and that a complete rotating magnetic field will also be generated in the ferrite by the eigenvectors $\vec{u}_2$ or $\vec{u}_3$. The result shown, however, suggests that the magnitude of $L_1$ is small but significant. In addition, referring to (7), it can be seen that the saturation magnetization of $L_2$ and $L_3$, as given by the numerators in the parentheses in (9), have also exhibited smaller values than the material saturation magnetization of 1200 Gauss.

### B. Physical Interpretation by Magnetic Flux Observation

To clarify these differences between the ideal and experimental results, the flux generated by the parallel circulator driving line was observed using a DC scale model of the line, which mimics the same flux distribution as that in a lumped element circulator. The apparatus employed, consisting of the scale model and a magnetic flux visualizer, are shown in Fig. 4, together with a simulated flux image for eigenvector $\vec{u}_1$.

The flux visualizer is constructed using iron oxide powder in a liquid suspension. The powder congregates in the parts

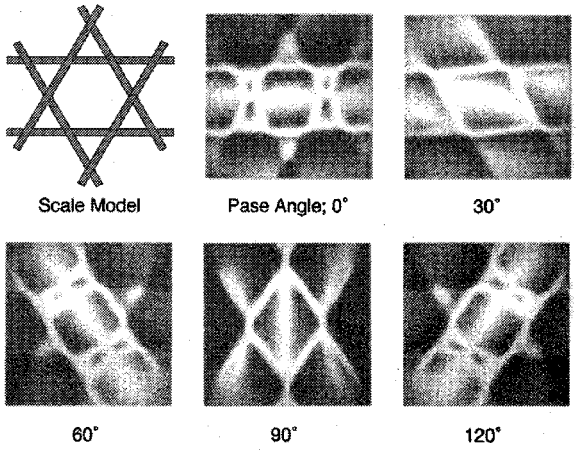


Fig. 5. Rotating magnetic flux of parallel line.

of the model where the magnetic flux is perpendicular to the visualizer. Hence, in the dark parts in the figure, magnetic flux will be perpendicular to the visualizer, while light parts will correspond to either a weaker flux area or an area in which the flux is parallel to the visualizer. The flux image of $\vec{u}_1$ suggests that the area of no flux defined in the original theory is restricted to a hexagonal area surrounded by the three pairs of parallel lines. Parallel flux is seen to flow in the light areas surrounding the hexagon, as illustrated by arrows in the flux image of $\vec{u}_1$. This image led to the conclusion that the nonnull value of $L_1$ is due to the stray inductance of an external area surrounding the hexagon. Hence an inductor should be connected in series to each inductor in the equivalent circuit illustrated in Fig. 1, to account for this effect.

The process of flux observation may be extended using a magnetic flux viewer to observe the magnetic flux distribution for $\vec{u}_2$ and $\vec{u}_3$, by applying the appropriate instantaneous value of a rotating three phase current to the three driving lines. The simulated flux images for $\vec{u}_2$ and $\vec{u}_3$ are the same, except for the sense of rotation. Fig. 5 shows images of flux for phase angle steps of 30°, covering one third of a rotation cycle. The images show that a clear view of flux rotation is observed only in the same hexagon found in the image of $\vec{u}_1$. This fact suggests that the smaller than expected experimental values of the saturation magnetization, given in (9), come from a rotating flux in the restricted hexagon alone, while the external area surrounding the hexagon behaves like a series connected inductor, as discussed in the $L_1$ case above.

### C. Driving Line Structure Design

The eigenvalue of inductance of two typical driving line structures, shown in Fig. 6, were evaluated with a view to optimizing the isolation bandwidth of the MC$^3$. The first, and more complicated structure, consists of three woven symmetric parallel lines, as used in the experiment above. The other comprises three stacked single lines with a simpler structure. The inductances of the two models were evaluated at 800 MHz as shown in (a) and (b) of Fig. 7, respectively. The isolation bandwidth was calculated from a bandwidth factor $\eta$, which depends upon the inductances $L_2$ and $L_3$, as per (6). The $\eta$ of each of the two line structures was calculated, as shown

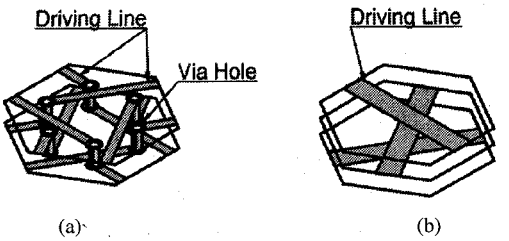


Fig. 6. Decomposed structure of driving line. (a) Woven parallel line. (b) Stacked single line.

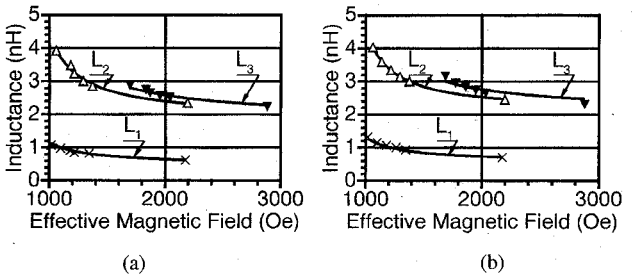


Fig. 7. Inductance of parallel line and single line. (a) Parallel line. (b) Single line.

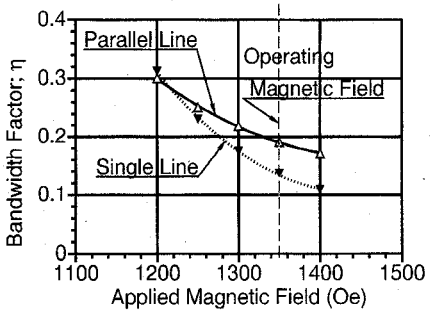


Fig. 8. Bandwidth factor comparison of line structure.

in Fig. 8, utilizing the best fit curves of the experimentally obtained inductances. Since a higher value of $\eta$ is favorable to obtain a broader isolation bandwidth, the difference in $\eta$ discriminates between the two line structures. The result shows that the $\eta$ of the parallel line is 30% higher than that of the single line at a magnetic field of 1350 Oe, applied to a conventional circulator exhibiting magnetic loss free operation. Hence the parallel line element will exhibit a 30% wider isolation bandwidth than that of the single line element.

The rotating magnetic flux image for the single line element was also observed, as shown in Fig. 9. An unclear image in this case means that the area of complete flux rotation is smaller than for the parallel line. The smaller value of $\eta$ of the single line results from this more restricted area of completely rotating flux.

Referring to the flux images above and evaluated inductance, a great deal of effort has been devoted to the determination of a optimum driving line structure formula, as a function of the dimensions of the driving line. However, a complex relationship between the area of the inner hexagon and the area of the external magnetic path prevented the derivation of a simple formula. Hence, an optimum driving line structure could only be selected from the experimental data.

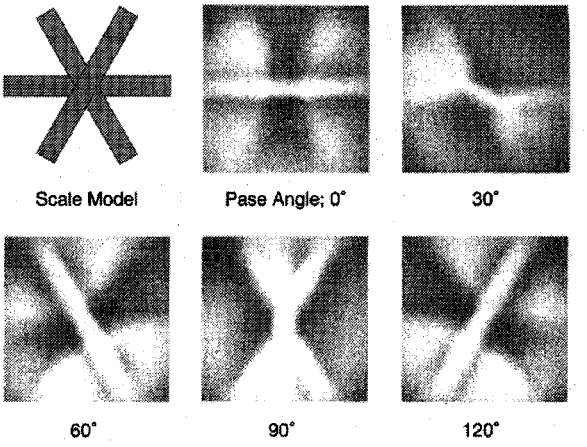


Fig. 9. Rotating magnetic flux of single line.

## IV. Preparation of Circulator Element

### A. Construction of Conductors in Ferrite

The MC$^3$ is fabricated using conventional multilayer technology, combined with novel methods for the construction of the driving line conductors [1].

As has been described, the embedding of conductors in the ferrite element is necessary to avoid a demagnetizing field, however, it was previously considered that a high ferrite sintering temperature would prevent such embedding. Two novel methods have overcome this difficulty. The first, called the melted metal method, employs the sintering of conductor paste embedded within unsintered sheet laminate. Since the paste is embedded in the laminate, it will remain within the sheet during conductor sintering and driving line conductors will be formed during subsequent cooling.

In the case of the second, paste intrusion, method hollows are created within the sheet laminate by first printing dummy conductors onto presintered sheets using carbon paste. The carbon paste dissipates during the ferrite sintering process leaving hollows in the circulator element. Silver paste is then intruded into the hollows using an isostatic press and then the complete element is fired at a temperature lower than the melting point of the silver, which remains within the circulator element. A similar method for the intrusion of molten metal instead of silver paste is well known in ceramic capacitor technology.

X-ray micro-focus photographs and cross-sectional secondary emission microscope (SEM) images of conductors constructed by the two methods described above are shown in Fig. 10. White spots observed in the photograph of a conductor produced by the melted metal method are pores caused by the formation of oxygen foam in the melted silver at the solidifying point. Such pores have seriously reduced the production yield of ferrite elements prepared by this method.

In the case of a conductor prepared using the paste intruding method, an air gap between the ferrite and the conductor can be seen in the cross-sectional SEM image. This gap is formed naturally during the firing process of the silver paste and is undesirable in the case of ceramic capacitor technology. However, since the gap has no influence on the generation of magnetic flux it is possible to adopt this method for the MC$^3$.

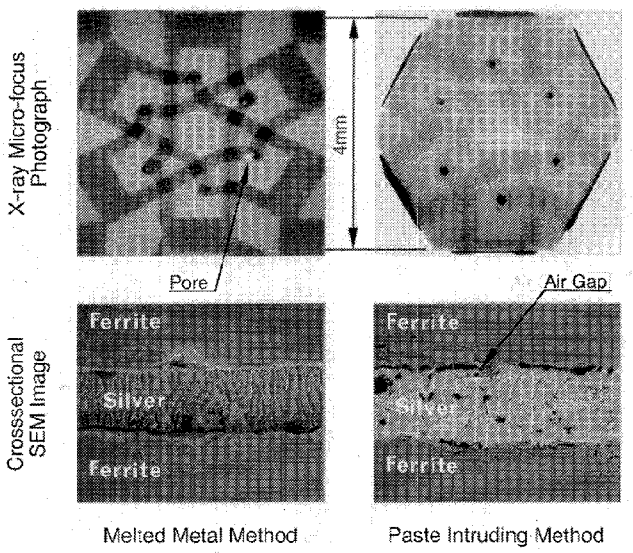


Fig. 10. X-ray micro-focus photograph and crosssectional SEM image of conductor.

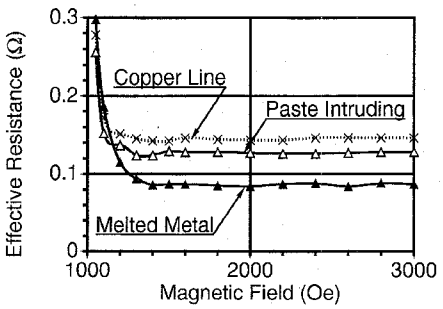


Fig. 11. Resistance of conductors.

### B. Conductor Resistivity Evaluation

The resistivity of a circulator driving line conductor is directly related to the insertion loss of the circulator. The resistivity of various conductor types was determined by evaluating the effective resistance of circulator elements, using a $Q$-factor measurement of the circulator element in a magnetic field. With a sufficiently strong magnetic field, the magnetic loss of an element vanishes and only the resistivity of the conductor remains. The resultant resistances for various applied magnetic field strengths are compared in Fig. 11, for elements constructed using the melted conductor method, intruded silver paste method and a copper strip line, as used in a conventional circulator. The silver paste intruding method gave a smaller resistance than of a copper line, while an element formed using the melted conductor method had the smallest resistivity, despite the formation of pores in the conductor.

## V. Circulator Characteristics

A decomposed structural view and an external view of the inductive circulator element are also shown in Fig. 12. An expanded external view of a completed $MC^3$ isolator element and a photograph of the isolator are shown in Fig. 13(a) and (b), respectively. In order to achieve a broad isolation bandwidth with high manufacturing yield, a parallel driving

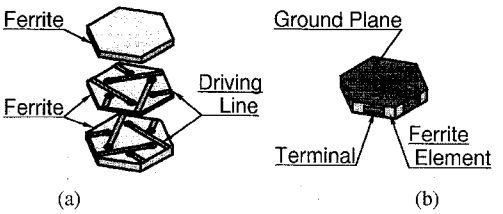


Fig. 12. Structure and external view of element. (a) Decomposed structure. (b) External view.

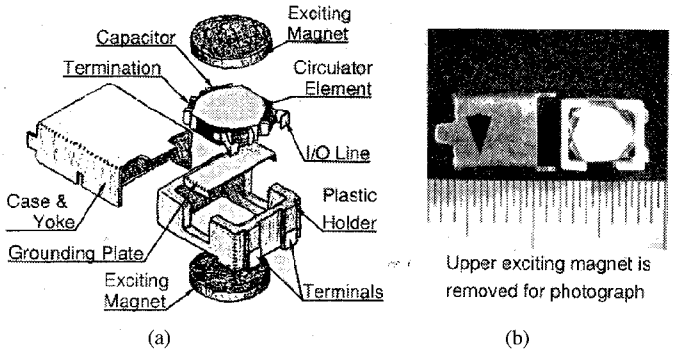


Fig. 13. Structure of $MC^3$ isolator. (a) Decomposed structure of $MC^3$ isolator. (b) Photograph of $MC^3$ isolator.

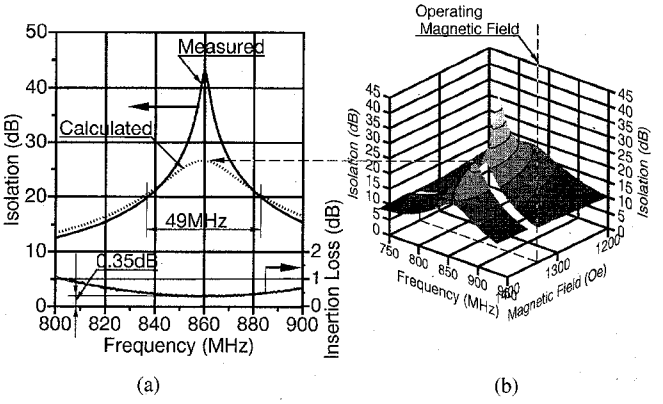


Fig. 14. Transmission characteristics of $MC^3$ isolator. (a) Transmission characteristics. (b) Calculated isolation characteristic.

line was constructed by the silver paste intrusion method. The circulator element was installed in a steel housing along with resonance capacitors, a termination resistor and a pair of exciting permanent magnets. The dimensions of the model are 6 mm, 6 mm and 3 mm in length, width and height, respectively. Both the number of parts and the amount of production processing employed in the $MC^3$ were greatly reduced, to a level approximately half that of a conventional circulator.

The transmission characteristics of the isolator are shown in Fig. 14(a). A measured isolation bandwidth of 49 MHz in the 800 MHz range, corresponding to a 5.8% relative bandwidth, was approximately 29% wider than that of a conventional circulator of this size, the TDK CU-406 [8]. A minimum insertion loss of 0.35 dB was obtained.

A calculated isolation characteristic, determined by substituting measured inductances into the equations discussed

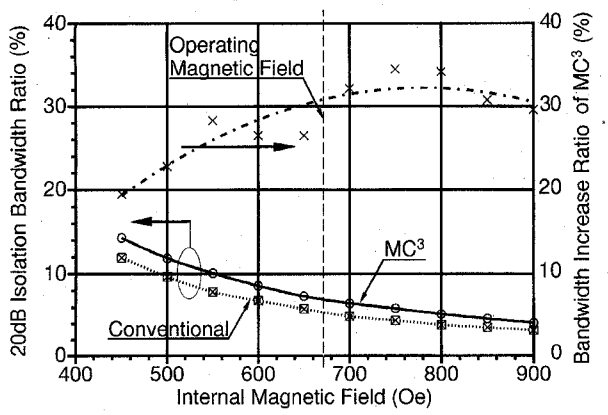


Fig. 15. Theoretical bandwidth comparison.

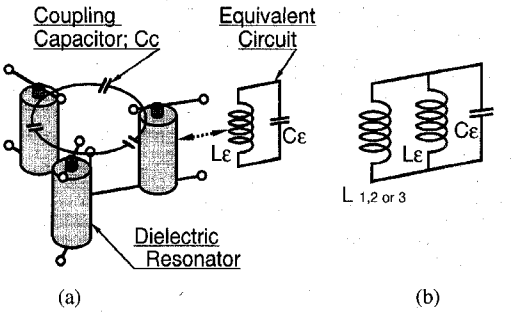


Fig. 16. Measuring apparatus of inductance eigenvalue. (a) Construction of measuring apparatus. (b) Equivalent circuit of resonator with circulator.

earlier is also plotted in Fig. 14(b), against magnetic field and frequency. The dotted line in Fig. 14(a) is a theoretical isolation characteristic for this circulator transposed from the operating magnetic field plane of Fig. 14(b). Although certain adjustments were made to the resonating capacitors, agreement between theoretical 20 dB isolation bandwidth and measured results was good. The significant deviation observed at maximum isolation is caused by a small difference in load matching conditions. Experiments have shown that such a difference has little effect on the isolation bandwidth.

The theoretical isolation bandwidth was also evaluated for the conventional circulator mentioned above. The difference between the theoretical performance of this and the MC³ is shown in Fig. 15 in terms of the 20 dB isolation bandwidth, calculated by (6), and the ratio of the bandwidth of each device. This result shows that the isolation bandwidth of the MC³ is approximately 30% wider than that of the conventional circulator and thus theoretically confirms the broader bandwidth of the MC³. A detailed relationship between the theoretical isolation bandwidth and the RF magnetic circuit structure will be discussed at a later date.

## VI. Conclusion

A circulator having a continuous RF magnetic circuit, abbreviated as MC³, has been developed by combining conventional multilayer ceramic technology and novel methods for embedding conductors in the circulator element. This continuous magnetic circuit was realized in order to construct an ideal circulator, and was achieved by the removal of the RF demagnetizing field associated with conventional circulators. Measurements of the transmission characteristics of the new circulator have demonstrated the validity of a design theory based on eigenvalue evaluation. The obtained 20 dB isolation bandwidth of 5.8% at 800 MHz exceeded the bandwidth of a conventional circulator of the same size by 29% and the insertion loss of 0.35 dB was less than the level normally associated with a conventional circulator. The greatly simplified production process for the MC³ will also enable a significant reduction in circulator cost.

With the rapid increase in the use of mobile telephone sets, power amplifier run-away or a reduction in carrier-to-noise ratio (C/N) caused by the counter flow of RF power from nearby telephone sets may become a serious problem. The insertion of a circulator between the antenna and power amplifier is one of the most effective countermeasures. However, the large size and high price of conventional circulators have until now prevented their installation in telephone sets. It is expected that MC³ with its small size, broadband characteristics and inexpensive production will thus make a major contribution to the stabilization of RF circuits in mobile telephone sets.

Further integration, such as the incorporation of capacitors or co-firing with exciting magnets, will also be possible. We however believe that, in view of slow progress in present ceramic technology, the MC³ has already become the preferred structure for lumped element circulators.

## Appendix
## Measuring Method for Inductance Matrix Eigenvalues

Three equally coupled resonators, as shown in Fig. 16(a), have two angular resonance frequencies $\omega_{0s}$ and $\omega_{0r}$. The former is the resonance for the eigenvector $\vec{u}_1$ and corresponds to a synchronous phase excitation of the resonators. The angular resonance frequencies for the eigenvectors $\vec{u}_2$ and $\vec{u}_3$ are degenerated to a single value of $\omega_{0r}$ that corresponds to both positive and a negative rotating phase excitations. If quarter wave length dielectric resonators are used, the equivalent circuit of the unit resonator is as given in (A1), based on the resonator characteristic impedance $Z_\varepsilon$ and the angular resonance frequency $\omega_\varepsilon$ of a single resonator.

$$C_\varepsilon = \frac{\pi}{4Z_\varepsilon\omega_\varepsilon}, \quad L_\varepsilon = \frac{4Z_\varepsilon}{\pi\omega_\varepsilon}. \tag{A1}$$

The above resonance frequencies $\omega_{0s}$ and $\omega_{0r}$ may be described, as given in (A2), by the equivalent inductance $L_\varepsilon$, the equivalent capacitance $C_\varepsilon$ and the coupling capacitance $C_c$.

$$\left.\begin{aligned} \omega_{0s} &= \frac{1}{\sqrt{L_\varepsilon C_\varepsilon}} \\ \omega_{0r} &= \frac{1}{\sqrt{L_\varepsilon(C_\varepsilon+3C_c)}} \end{aligned}\right\}. \tag{A2}$$

When the inductive part of a lumped element circulator is connected to a coupled resonator, the equivalent circuit of the resonator changes, as shown in Fig. 16(b). The gyromagnetic characteristics of the circulator remove the degeneracy of $\vec{u}_2$ and $\vec{u}_3$, producing instead three angular resonance frequencies $\omega_i$ (where $i = 1, 2$, and 3), corresponding to excitation by the corresponding eigenvectors. The inductances $L_1, L_2$, and $L_3$ may thus by calculated by (A3) from the three angular resonance frequencies, coupling capacitors $C_c$ and equivalent capacitance $C_\varepsilon$.

$$\left.\begin{aligned} L_1 &= \frac{1}{C_\varepsilon\left(\omega_1^2-\omega_{0s}^2\right)} \\ L_{2 \text{ or } 3} &= \frac{1}{(C_\varepsilon+3C_c)\left(\omega_{2 \text{ or } 3}^2-\omega_{0r}^2\right)} \end{aligned}\right\}. \tag{A3}$$

## ACKNOWLEDGMENT

The authors would like to express their appreciation for the invaluable advise of A. Nabae of Tokyo Institute of Polytechnics. They would like to express their thanks to the research group members of TDK Corporation Materials Research Center for their stimulating discussions and for the preparations of samples. Also, the authors are indebted to M. Chinn for his helpful contributions to the preparation of this paper. Finally, the support of Executive Managing Director T. Masaki of TDK Corporation is gratefully acknowledged.

## REFERENCES

[1] T. Miura and Y. Konishi, "New lumped element circulator by ceramic integrated circuit technology," *IEEE Trans. Broadcasting*, vol. 41, no. 3, pp. 101–106, 1995.
[2] H. Nagata and Y. Konishi, "New measuring method of eigenvalues of nonreciprocal three ports network," *Tech. Rep. IEICE*, MW 95–108, pp. 79–84, 1995 (in Japanese).
[3] M. Kobayashi, K. Kawamura, and K. Suzuki, "High $Q$-factor tri-plate resonator with an inner conductor of melted silver," *Ceramic Trans.*, vol. 41, pp. 355–362, 1994.
[4] J. A. Weiss, G. F. Dionne, and D. H. Temme, "The ring-network circulator for integrated circuits: Theory and experiments," *IEEE Trans. Microwave Theory Tech.*, vol. 13, no. 6, pp. 852–864, 1965.
[5] Y. Konishi, "Lumped element $Y$ circulator," *IEEE Trans. Microwave Theory Tech.*, vol. 13, no. 6. pp. 852–864, 1965.
[6] T. Miura, M. Kobayashi, H. Nagata, and Y. Konishi, "Optimization of a lumped element circulator based on eigen inductance evaluation and structural improvement," *IEEE MTT-S Int. 1996 Microwave Symp. Dig.*, 1996, pp. 117–120.
[7] D. Polder, "On the theory of ferromagnetic resonance," *Phil. Mag.*, vol. 40, no. 2, pp. 99–115, 1949.
[8] TDK Corporation of America, 1600 Feehanville Drive, Mt. Prospect, IL 60056.

**Taro Miura** was born in Tokyo, Japan, on July 21, 1938. He received the B.E. degree from Keio University, Tokyo, Japan, in 1962.

Since 1962 he has been with the Research and Development Laboratory of TDK Corporation, Ichikawa, Chiba, Japan where he was in the development of microwave devices applying gyromagnetic materials until 1979. Since then he was engaged in the development of RF absorbers backed up with ferrite tiles and in the design of anechoic chambers installing these absorbers until 1990 in the RF Absorber Manufacturing Division. He transferred to the Material Research Center of TDK Corporation, Narita, Chiba, Japan for the evaluation of microwave materials and the development of a lumped element circulator. He is presently responsible for the development of RF elements at the Advanced Products Development Center of TDK Corporation, Ichikawa, Chiba, Japan.

**Makoto Kobayashi** was born in Tokyo, Japan, in 1949. He received the B.S. and the M.S. degrees in chemistry from Sophia University, Tokyo, Japan, in 1973.

Since 1973 he has been with the Research and Development Laboratory of TDK Corporation, Ichikawa, Chiba, Japan, where, he was in the development of anode coating materials for caustic soda electrolysis until 1982. Since then he has developed co-precipitation method of ceramic dielectric materials. He is presently a group leader of the development of microwave dielectric and magnetic materials in the Materials Research Center of TDK Corporation, Narita, Chiba, Japan.

Mr. Kobayashi is a Member of the Chemical Society of Japan.

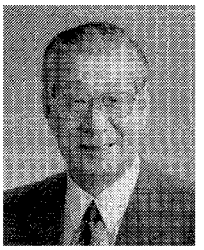

**Yoshihiro Konishi** (F'81) was born on September 24, 1928 in Nara, Japan. He received the B.Eng. and the Ph.D. degrees in engineering from Kyoto University, Japan in 1951 and 1961 respectively.

He joined Nippon Hoso Kyokai (NHK) in 1951. From 1962 to 1963 he was a visiting scholar at the Microwave Research Institute of Polytechnic Institute of Brooklyn. He was a project manager for joint experiments for the development of a Satellite Earth Station conducted by NHK Technical Research Laboratories. In November of 1983 he joined Uniden Corporation where he was Senior Executive Vice President. In 1993 he retired from Uniden Corporation, and is Professor of Tokyo Institute of Polytechnics.

Dr. Konishi received the Medal with Purple Ribbon from the Japanese Emperor in 1982. Among other awards, he received the award of the Minister of the Post Office (1978), the award of the Minister of the Patent Bureau (1977) and the award of the Minister of the State for Science and Technology (1979). He received 1994 Carrier Award of IEEE Microwave Theory and Techniques Society. He is a Senior Editor for Asia for the IEEE Society on Broadcast Technology. He is registered in the *Who's Who in America* as an electromagnetic scientist.